Assessment of Unsteady-RANS Approach against Steady-RANS Approach for Predicting Twin Impinging Jets in a Cross-Flow

Zhiyin Yang

Department of Engineering and Design University of Sussex, Brighton BN1 9RH, UK

Abstract: A complex flow field is created when a vertical/short take-off and landing (VSTOL) aircraft is operating near ground. One major concern for this kind of aircraft in ground effect is the possibility of ingestion of hot gases from the jet engine exhausts back into the engine, known as hot gas ingestion (HGI), which can increase the intake air temperature and also reduce the oxygen content in the intake air, potentially leading to compressor stall, low combustion efficiency and causing a dramatic loss of lift. This flow field can be represented by the configuration of twin impinging jets in a cross-flow. Accurate prediction of this complicated flow field under the Reynolds Averaged Navier-Stokes (RANS) approach (current practise in industry) is a great challenge as previous studies suggest that some important flow features cannot be captured by the Steady-RANS (SRANS) approach even with a second order Reynolds Stress Model (RSM). This paper presents a numerical study of this flow using the Unsteady-RANS approach (URANS) with a RSM and the results clear indicate that the URANS approach is superior than the SRANS approach but still the predictions of Reynolds stress are not accurate enough.

Key words: Twin impinging jets, URANS, SRANS, HGI.

Nomenclature

d	[m]	Jet diameter
H	[m]	Channel height
U	[m/s]	Streamwise (horizontal, x direction) velocity
V_j	[m/s]	Jet velocity (vertical, y direction)
k	[kgm^2/s^2]	Turbulent kinetic energy
u'	[m/s]	Fluctuating component of streamwise velocity
v'	[m/s]	Fluctuating component of vertical velocity
u'^2	[m^2/s^2]	Normal stress in streamwise direction
v'^2	[m^2/s^2]	Normal stress in vertical direction
$u'v'$	[m^2/s^2]	Shear stress
x	[m]	Cartesian axis direction
y	[m]	Cartesian axis direction
z	[m]	Cartesian axis direction

Special characters

ε	[kgm^2/s^3]	Turbulent kinetic energy dissipation rate

Subscripts

j	Jet

1. Introduction

When a vertical/short take-off and landing (VSTOL) aircraft is operating close to the ground a complicated flow field is generated underneath it. This flow field is 3D and has some distinct large scale unsteady flow structures such as ground vortex, up-wash fountain. The main area of concern is the possibility of ingestion of hot gases from the jet exhausts back into the engine, known as Hot Gas Ingestion (HGI). The HGI comes from the interaction of the impinging jet on a ground plane being re-circulated either in an up-wash fountain via encroachment along the aircraft to the intakes in the near field, or in the far field when there is a head wind. The head wind causes the flow along the ground to deflect upwards creating a vortex back towards the intakes. This will increase the intake air temperature and less content of oxygen, potentially leading to compressor stall and causing a dramatic engine thrust loss (Knowles & Bray, 1991; Li, Page & McGuirk, 2007). Studying twin impinging jets along the spanwise direction in a cross-flow is directly relevant to the understanding of this complicated flow field.

Early research into the effects created by a VSTOL aircraft started in the 1960s mainly through wind tunnel experiments (Cox & Abbot, 1966; MeLemore, Smith & Hemeter, 1970). The investigation concentrated on HGI and included tests of several exhaust-nozzle configurations at a range of heights and was conducted over a range of forward speeds. The HGI into the inlets was found to be dependent upon the aircraft configuration and wind speed. The configuration with the least amount of HGI was an ‘in-line’ twin nozzle, which is similar configuration to the new STOVL aircraft, the Joint Strike Fighter/F-35 by Lockheed. Nevertheless due to the limitation of experimental techniques at that time detailed measurements of flow field was not possible and hence the flow mechanisms were not fully understood.

A detailed experimental study (Barata, Durao, Heitor & McGuirk, 1991) was performed using a water flow rig with twin jets set up side by side and the experiment data have been used for validation in many numerical studies through the 1990's onwards. A Laser Doppler system was used to allow measurements of flow velocity components to be recorded. This allowed for analysis of the three dimensional flow field and shear stress distribution. Intense velocity fluctuations are observed in the shear layers surrounding the impingement regions from the jets and the upwash fountain. The latter of which are dominated by strong curvature effects. They also performed a numerical simulation of the same flow case using the standard k – ε model (Barata et al., 1991) and concluded that calculation of the turbulent structure of the shear layers requires consideration of the individual Reynolds stresses.

Another experimental study (Behrouzi & McGuirk, 1998) was also carried out in a water rig but with different configurations: case one had no cross-flow and equal jet velocities, case two had no cross-flow and unequal jet velocities, case three had a cross-flow and equal jet velocities. Their major conclusions were that large local turbulence intensity was observed in the fountain region in case one and the opposing ground sheet flows led to a region of dominant normal stress production.

A further experimental study (Behrouzi & McGuirk, 2000) carried out included intake geometry. Again, three test cases were performed, with test case one having no intake geometry present, just the two impinging jets. Test case two had the intake geometry present but there was no intake flow. Test case three had intake geometry present, and there was also an intake flow present. Their study identified the effect of the re-enforcement process, occurring when the ground sheets from both jets merge together, with the penetration of the jet-plane being less than the

Zhiyin Yang, reader; research fields: Computational Fluid Dynamics, Large-Eddy Simulation of Transitional and Turbulent Flow, Combustion, Heat Transfer. E-mail:zhiyin.yang@sussex.ac.uk

penetration of the ground sheet for the fountain plane for all measure velocity ratios.

Experiments on this kind of very complicated flow filed are usually very expensive and the experimental conditions/parameters that can be tested are limited and hence it is very important to develop computational tools for this kind of flow. Direct Numerical Simulation (DNS) is the most accurate approach for computing turbulent flows since it compute all turbulent motions directly but the computational cost is huge and it is impossible to use it for practical engineering flows even with the most powerful computers available. Large-Eddy Simulation (LES) computes large scale turbulent motions directly and the small scale motions are modelled. It is possible to employ LES for some practical engineering turbulent flows but it is still very expensive computationally. The current practice in industry is to employ the so called Reynolds Averaged Navier-Stokes (RANS) for computing engineering turbulent flows. Several numerical studies (Barata et al., 1991; Behrouzi & McGuirk, 1999; Chuang, Chen, Lii & Tai, 1992; Worth & Yang, 2006; Ostheimer & Yang, 2012) using the Steady-RANS (SRANS) approach have been carried out and generally speaking the gross flow features of the flow can be predicted adequately. However, those numerical studies did not capture the turbulent structure of the fountain flow and impingement regions at all since SRANS cannot really predict any turbulent structures. The predicted turbulent quantities are particularly poor and this paper reports a numerical study of twin impinging jets in a cross-flow employing the Unsteady-RANS (URANS) approach, comparing the URANS results against the experimental data (Barata et al., 1991) and the SRANS results, assessing the URANS performance in this flow case.

2. Mathematical Formulation

The governing equations are derived from the fundamental physical principles: conservation laws for mass, momentum and energy. These equations are fairly standard and hence will only very briefly be presented here for incompressible flow.

2.1 Steady-RANS Governing Equations

As mentioned before that among the numerical approaches DNS is the most accurate approach but very demanding computationally and for practical engineering calculations some kind of simplification has to be taken in order to get results within a reasonable time scale and this is the so called the Reynolds Averaged Navier-Stokes (RANS) approach. The governing equations are time-averaged in the RANS approach and hence the obtained results are time averaged quantities. In statistically stationary turbulent flows (average properties not changing with time so that the time derivative term disappears from the equations). The SRANS governing equations are as follows:

$$\frac{\partial \overline{U}_i}{\partial x_i} = 0 \tag{1}$$

$$\frac{\partial (\overline{U}_i \overline{U}_j)}{\partial x_j} = -\frac{1}{\rho}\frac{\partial \overline{P}}{\partial x_i} + \frac{\partial}{\partial x_j}\left[\nu \frac{\partial \overline{U}_i}{\partial x_j}\right] - \frac{\partial (\overline{u_i u_j})}{\partial x_j} \tag{2}$$

2.2 Unsteady-RANS Governing Equations

In not statistically stationary turbulent flows or turbulent flows with large unsteady flow structures as demonstrated below in Fig. 1 showing the time trace of the velocity at a point. In such a case the time derivative term should not disappear (the average in this case is better to be understood as ensemble average, or time average over a certain period of time between T_1 and T_2).

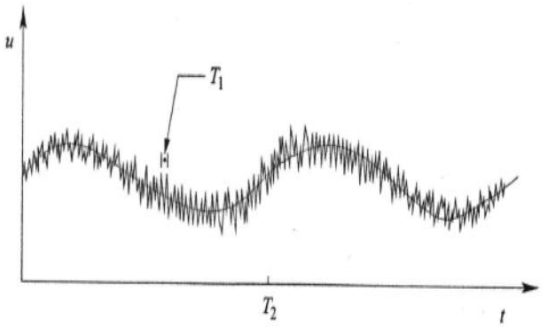

Fig. 1 Velocity at point in a not statistically stationary turbulent flows

Therefore the URANS governing equations are as follows:

$$\frac{\partial \overline{U}_i}{\partial x_i} = 0 \tag{3}$$

$$\frac{\partial \overline{U}_i}{\partial t} + \frac{\partial (\overline{U}_i \overline{U}_j)}{\partial x_j} = -\frac{1}{\rho}\frac{\partial \overline{P}}{\partial x_i} + \frac{\partial}{\partial x_j}\left[\nu \frac{\partial \overline{U}_i}{\partial x_j}\right] - \frac{\partial (\overline{u_i u_j})}{\partial x_j} \tag{4}$$

The averaging process introduces some unknown terms called Reynolds stresses (the last term on the right hand side of equations (2) and (4)), which have to be provided by a turbulence model before the governing equations can be solved. There have been many turbulence models developed so far and the current study employs one of the most advanced turbulence model, Reynolds Stress Model (RSM), which solves the Reynolds stresses using transport equations, rather than approximating them using other methods such as an eddy viscosity approach (e.g. *k-ε* model).

2.3 Reynolds Stress Model

The Reynolds stress transport equations can be derived from the Navier-Stokes equations and can be expressed as follows (neglecting body force and rotation force):

$$\frac{\partial (\overline{u_i u_j})}{\partial t} + \frac{\partial (\overline{U}_k \overline{u_i u_j})}{\partial x_k} = -\left[\overline{u_i u_k}\frac{\partial \overline{U}_j}{\partial x_k} + \overline{u_j u_k}\frac{\partial \overline{U}_i}{\partial x_k}\right] + \frac{\partial}{\partial x_k}\left[\nu \frac{\partial \overline{u_i u_j}}{\partial x_k} - \overline{u_i u_j u_k} - \overline{\frac{p}{\rho}(u_i \delta_{jk} + u_j \delta_{ik})}\right] + \overline{\frac{p}{\rho}\left[\frac{\partial u_i}{\partial x_j} + \frac{\partial u_j}{\partial x_i}\right]} - 2\nu \overline{\frac{\partial u_i}{\partial x_k}\frac{\partial u_j}{\partial x_k}} \tag{5}$$

The two terms on the left hand side of the equation are the time derivative term and convection term. On the right hand side of the equation the first term represents the production by mean flow deformation; the second term represents diffusive transport due to three contributions: molecular, turbulent and pressure diffusion; the third one is the pressure-strain term, accounting for stress redistribution due to fluctuating pressure; the fourth term is the dissipation term. Several terms in this exact transport equation need to be modelled. The turbulent diffusive transport term is modelled using a simplified version of the generalized gradient diffusion model proposed by Daly and Harlow (1970) to improve stability.

$$D_{T,ij} = \frac{\partial}{\partial x_k}\left[\frac{\mu_t}{\sigma_k}\frac{\partial (\overline{u_i u_j})}{\partial x_k}\right] \tag{6}$$

Gibson and Launder (1978) proposed the following pressure-strain model for the pressure-strain term (the third term on the right hand of equation (5)) using the classical decomposition approach consisting of three parts: the slow pressure-strain term, the rapid pressure strain term and the wall reflection term.

$$\phi_{ij} = \phi_{ij,1} + \phi_{ij,2} + \phi \tag{7}$$

$$\phi_{ij,1} = -C_1 \rho \frac{\varepsilon}{k}\left[\overline{u_i u_j} - \frac{2}{3}\delta_{ij} k\right]$$

$$\phi_{ij,2} = -C_2\left[(P_{ij} + C_{ij}) - \frac{2}{3}\delta_{ij}(P - C)\right]$$

$$\phi_{ij,w} = C_1'\left[\overline{u_k u_m} n_k n_m \delta_{ij} - \frac{3}{2}\overline{u_k u_i} n_k n_j - \frac{3}{2}\overline{u_k u_j} n_k n_i\right]\frac{0.4k^{1/2}}{d}$$
$$+ C_2'\left[\phi_{km,2} n_k n_m \delta_{ij} - \frac{3}{2}\phi_{ik,2} n_k n_j - \frac{3}{2}\phi_{jk,2} n_k n_i\right]\frac{0.4k^{3/2}}{\varepsilon d}$$

Where C_1=1.8, C_2=0.60, C'_1=0.5, C'_2=0.3, d is normal distance to the wall. P_{ij} and C_{ij} are the production and the convection terms in equation (3), C=1/2C_{kk}, P=1/2P_{kk}. The Gibson and Launder pressure-strain model is very popular and has been well tested in many cases, and hence is chosen here.

The modelled transport equation for the dissipation rate is:

$$\frac{\partial(\varepsilon)}{\partial t} + \frac{\partial(\varepsilon \overline{U}_i)}{\partial x_i} = \frac{\partial}{\partial x_i}\left[(\nu + \frac{\nu_t}{\sigma_\varepsilon})\frac{\partial \varepsilon}{\partial x_i}\right] + \frac{1}{2} C_{\varepsilon 1} P_{ii} \frac{\varepsilon}{\rho k} - C_{\varepsilon 2}\frac{\varepsilon^2}{k} \quad (8)$$

Where σ_ε=1.0, $C_{\varepsilon 1}$=1.44, $C_{\varepsilon 2}$=1.92.

2.4 Computational Details

The current study has been carried out using the commercial FLUENT code which uses the finite volume method and details are widely available. FLUENT offers a choice of two different numerical method based solvers, pressure based and density based. In the current study since water is used as the working fluid so that flow is incompressible. Hence the pressure based approach is used and the SIMPLE algorithm is employed for pressure-velocity coupling. The second order upwind scheme is used for the spatial discretization and a 2nd order implicit scheme for the temporal discretization. The wall treatment of combining a two-layer model with enhanced wall functions which blends linear and logarithmic laws-of-the-wall smoothly is employed. A Reynolds Stress Model (RSM) with the Gibson and Launder (1978) pressure-strain model as described above has been used.

The computational study tries to match the experiment (Barata et al., 1991) as closely as possible. The water channel within the flow rig where the experiments took place was 1.5m long, 0.5m wide and 0.1m high. Results were obtained for a flow configuration of Re = 105,000 based on the jet inlet velocity and the jet hole diameter, with twin jets set up side by side and a jet to cross-flow velocity ratio of 30. Figs. 2 and 3 show top and isometric views of the computational domain (the computational domain is divided into different blocks as shown by the internal lines for multi-block mesh generation) with the jet spacing of 5d, channel width of 25d and channel height of 5d, matching the experimental geometry exactly, all based on the jet hole diameter d=0.02m. The co-ordinates origin is located at the centre between the two jets on the channel top surface corresponding to the location as in the experiments with x-streamwise direction (cross flow direction), y-vertical direction (jet flow direction) and z-spanwsie direction. The upstream and downstream sections were lengthened to guarantee full capture of the ground vortex upstream of the jets and to ensure complete capture of the downstream behaviour of the flow, and also to match the previous SRANS geometry to allow comparisons between the URANS results and the SRANS results.

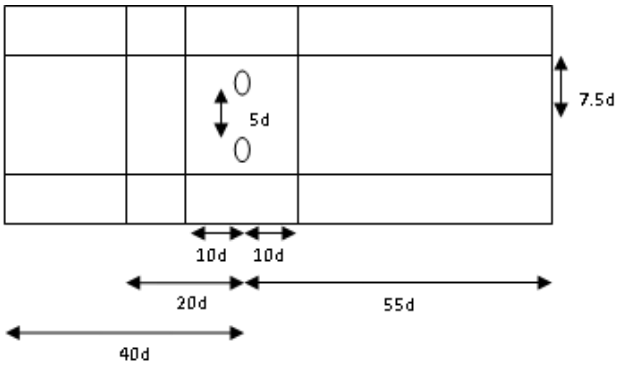

Fig. 2 Top view of the computational domain which is divided into multi-block for mesh generation

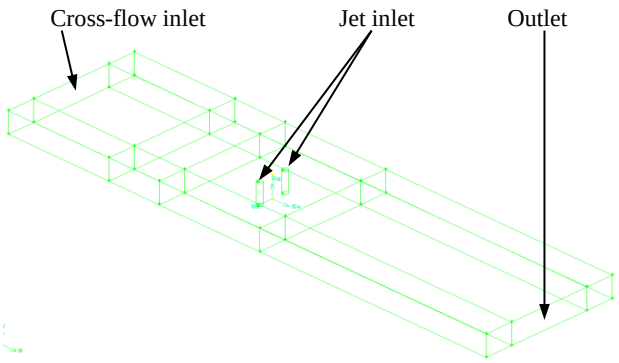

Fig. 3 Isometric view of the computational domain

Fig 4 shows a top view of the mesh used in the current study with refined cells in the jet regions and near the walls to ensure that there is good grid resolution around the impingement area of the flow. In most blocks, the structured mesh was used in order to achieve better numerical accuracy, except around the jet region where an unstructured mesh was used to better capture the circular jet geometry. The cell spacing in the upstream and downstream sections is slightly larger than that within the central section, as less detail is required to gather the flow features and behaviour within these regions. Three separate meshes were generated and mesh sensitivity studies were carried out to make sure that the solution is mesh independent. It was found that when mesh points were above 1.5 million there was hardly any change in the results. Hence the final mesh used in the current study has a total number of 1,755, 680 cells. In terms of the computational cost the URANS calculations was about 5 times more expensive than the SRANS calculations

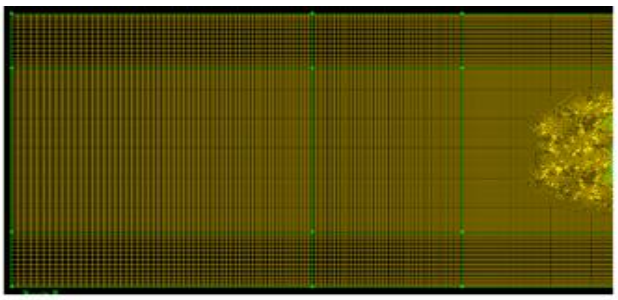

Fig. 4 Top view of the mesh

Table 1 Details of inlet boundary conditions

Variables	Values
Cross-flow inlet velocity	0.176 m/s
Jet flow inlet velocity	5.28 m/s
Cross-flow inlet k	9.09×10^{-7} m^2/s^2
Jet flow inlet k	5.94×10^{-4} m^2/s^2
Cross-flow inlet ε	1.42×10^{-8} m^2/s^3
Jet flow inlet ε	1.4×10^{-11} m^2/s^3
Cross-flow inlet normal stresses	6.06×10^{-7} m^2/s^2
Jet flow inlet normal stresses	3.96×10^{-4} m^2/s^2
Turbulent shear stresses at both inlets	0

2.4 Boundary conditions

The Reynolds number in the current study is the same as in the experiment (105,000) based on the jet inlet velocity and the jet hole diameter. Uniform jet and cross-flow velocities of 5.28m/s and 0.176 m/s respectively were worked out accordingly and applied at the inlet boundaries. Values of turbulent kinetic energy and dissipation rate (k, ε) and normal stresses at jet and cross-flow inlets were derived from the measured turbulent intensities and the estimated length scales while the shear stresses were assumed to be zero. A preliminary study on inlet boundary condition sensitivity was also carried out, especially with different assumed shear stress values, and the results were very similar with only about 3% difference between zero shear stress and non-zero shear stress values.

Details of the inlet boundary conditions are given in table 1. A zero gradient boundary was applied at the outlet. No slip wall boundary condition was applied at all other boundaries (top, bottom and side walls).

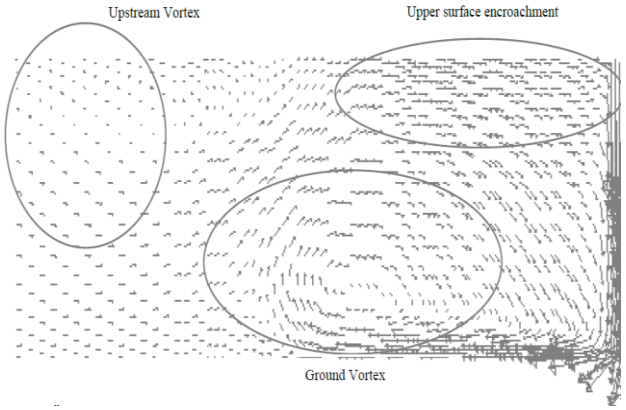

Fig. 4 URANS: jet plane velocity vectors (left jet)

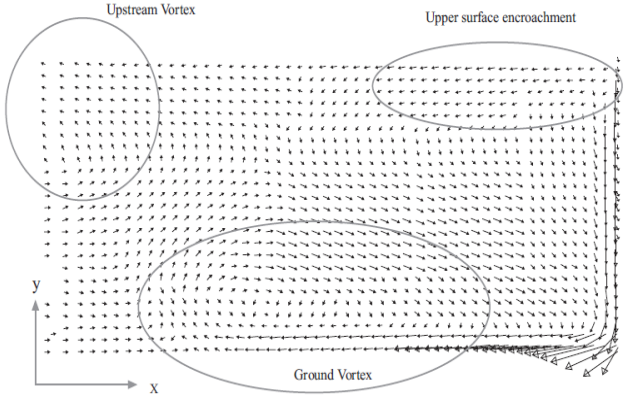

Fig. 5 SRANS: jet plane velocity vectors (left jet)

3. Results and Discussion

Figs. 5 and 6 show the URANS and SRANS velocity vectors upstream of the jet locations in the jet plane (the x-y plane cutting through the jet centre). Three main flow features are visible from both the URANS and SRANS results: The ground vortex resulting from the ground sheet flow from the fountain interacting with the cross-flow; fluid encroachment along the upper surface as a result of the fluid entering the flow from the jets; and a vortex upstream of the ground vortex, located near the upper surface of the channel. The predicted gross flow features by both the URANS and SRANS are very similar although the ground vortex centre from the URANS results seem to be slightly higher than that of the SRANS results and also slightly stronger fluid entrainment near the jet is predicted by the URANS approach. Detailed analysis reveals that the URANS prediction of the ground vortex length and location is better when compared with the experimental data than those of the SRANS predictions. The predicted ground vortex length by the URANS approach is 9.4d while it is about 9.2d by the SRANS approach and the measured one is about 9.5d (the ground vortex length is defined here as the distance between tip of the ground vortex to center of the jet, and vortex tip is defined as the point where the axial velocity is zero).

Fig. 7 presents the comparison between the predicted mean horizontal velocity profiles along the vertical direction by both the URANS and the SRANS approaches, and the experimental data at five streamwise locations (velocity is normalized by the jet velocity, H is the channel height) in the central plane (x,y). Generally speaking the predictions by both approaches follow the trend of the experimental results quite well but the URANS method performed better than the SRANS method as the URANS results are closer to the experimental data at all locations except at x/d=-1.5. This is just upstream of the jet which is an important area of the flow as it affects the size and location of the upstream ground vortex. The URANS simulation shows better agreement with the experimental data at locations downstream of the impingement, especially at x/d=1.5 and 4 the URANS results are very close to the experimental data. However both approaches appears to under-predict the influence of horizontal velocity of the ground sheet created by the impinging jets in the lower regions of the flow.

Fig. 8 shows comparison between the predicted shear stress profiles and the experimental data in the central plane (x, y) at the same five stream streamwise locations as in Fig 7. Results by both the SRANS and

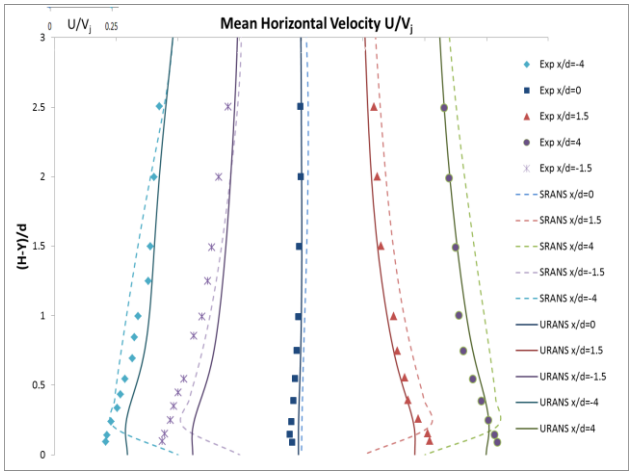

Fig. 7 Comparison between the predicted velocity profiles and the experimental data

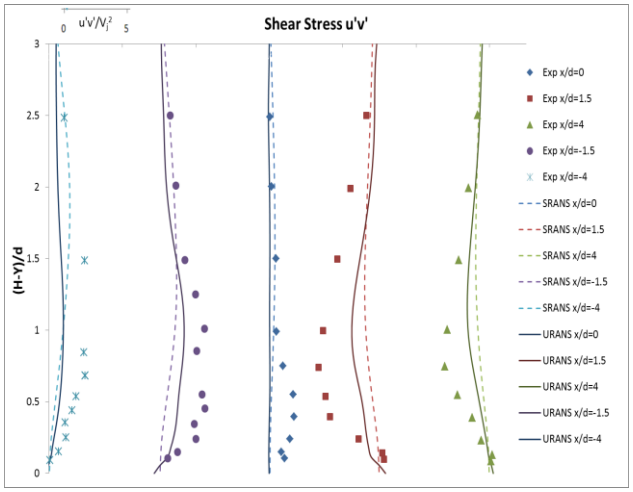

Fig. 8 Comparison between the predicted shear stress and the experimental data

URANS approaches follow the trend of the experimental data reasonably well and it can be seen clearly that the URANS results are closer to the experimental data, confirming again that the URANS approach performs better than the SRANS approach in this case. Nevertheless there are still some discrepancies between the experimental data and the URANS results, especially at x/d=0 there is a peak near the wall indicated by the experimental data whereas this peak is not predicted by both the SRNAS and URANS approaches.

Fig. 9 shows the horizontal velocity fluctuations (root mean squared, rms, normalized by the jet velocity square) in the centre plane (x, y) at the same five streamwise locations. It is apparent from the figure that when comparing against the experimental data the URANS results are much improved in terms of trend and accuracy apart from one location at x/d=0. The SRANS results do not even follow the trend of the experimental data, clearly indicating the superiority of the URANS approach over the SRANS approach for this flow case.

The comparison between the predicted vertical normal stress and the experimental data in the central plane (x, y) at the same five streamwise locations in Fig. 10 confirms the superiority of the URANS approach. Again the URANS results show a large improvement in trend and accuracy over the SRANS results. The URANS results follow the trend of the experimental data very well, particularly away from the impingement zone at two locations (x/d=-4 and x/d=4) the agreement between the predictions and the experimental data is excellent. The predicted profiles by the URANS approach near the ground plane also agree well with the experimental data at all five locations, in contrast to the streamwise normal stress predictions shown in Fig. 9 where the agreement is poor.

It is clear from the above discussion that the mean velocity filed is reasonably well predicted by both the URANS and the SRANS approaches with slightly better performance from the URANS approach.

However, it is a different story for the normal and shear stresses predictions. The URANS approach is much superior to the SRANS approach, especially for the vertical normal stress predictions as shown in Fig. 10 where the URANS results follow the trend of the experimental data very well, particularly at two locations (x/d = -4 and x/d = 4) the agreement between

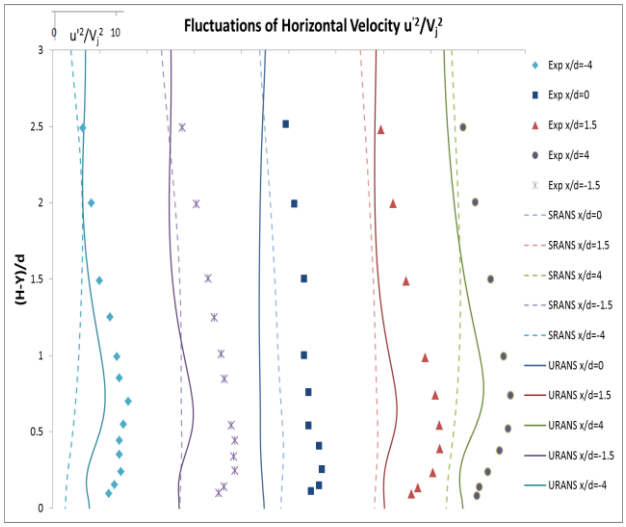

Fig. 9 Comparison between the predicted streamwise normal stress and the experimental data

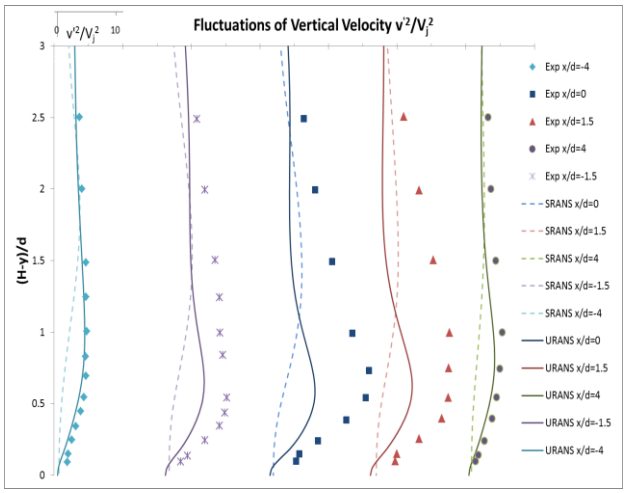

Fig. 10 Comparison between the predicted vertical normal stress and the experimental data

the URANS results and the experimental data is excellent. Whereas for the SRANS approach it can be seen clearly from the above figures that the prediction is very poor with a big discrepancy between the prediction and the experimental data. Not only the predicted stress magnitude is so much smaller but also the predicted stress profiles do not even follow the trend exhibited by the experimental results. The poor predictions of turbulent stresses by the SRANS approach are mainly due to the fact that the flow field is very complicated and dominated by several very large scale unsteady flow features (ground vortex, possible flapping of fountain vortices etc.) which the SRANS approach could not capture these unsteady large scale flow features accurately at all.

There are certain flow features such as the upwash fountain which are not predicted well by both approaches. It has been recognized that it poses considerable challenges to any modelling strategy for predicting the upwash fountain accurately due to the combination of impingement, jet collision and cross-flow.

4. Conclusion

A comparative CFD study of twin impinging jets through a cross-flow using two different approaches (the Steady-RANS and the Unsteady-RANS) with a Reynolds stress model has been presented in this paper. The flow field investigated is representative of the complex flow field underneath a vertical/short take-off and landing aircraft operating very close to the ground. It is important to assess the strengths and weaknesses of the computational tools (SRANS and URANS approaches) used currently for the practical engineering flows as DNS and LES are still far too computationally expensive.

Both the SRANS and the URANS performed well overall as far as the mean flow field is concerned, showing good trend of the experimental results as well as good accuracy, with slightly better predictions by the URANS approach. However, the SRANS approach performed very poorly in terms of Reynolds stress predictions whereas the URANS approach is clearly much superior, showed much improvement over the SRANS approach, producing results with much better agreement with the experimental data. In particular, for the vertical normal stress predictions as shown in Fig. 10 where the URANS results not only follow the trend

of the experimental data very well but also the quantitative agreement between the URANS results and the experimental data is very good. This strongly indicates that for the current flow case with large scale unsteady flow features the URANS approach is definitely better than the SRANS approach, and it could be concluded that the URANS approach is a better choice for any flow cases with large scale unsteady flow features. However, even the URANS approach fails to predict Reynolds stresses accurately which is mainly due to the fact that URANS may be able to capture some large scale unsteady flow motions but it cannot capture turbulence well. If detailed turbulent information is needed then it is only possible to employ LES.

Acknowledgement

This research work was carried out using the computing facilities at Loughborough University and I kindly acknowledge that the contributions of my former students: S.Webb-Martin who produced the URANS results and D. Ostheimer who produced the SRANS results.

References

Barata, J., Durao, D., M. Heitor, M., & McGuirk, J. J. (1991). Impingement of single and twin turbulent jets through a cross-flow. *AIAA Journal*, 29, 595-602. doi: 10.2514/3.10626

Behrouzi, P., & McGuirk, J. J. (1998). Laser doppler velocimetry measurements of twin-jet impingement flow for validation of computational models. *Optics and Lasers in Engineering*, 30, 265-277. doi: 10.1016/S0143-8166(98)00030-X.

Behrouzi, P., & McGuirk, J. J. (1999). Computational fluid dynamics prediction of intake ingestion relevant to short take-off and vertical landing aircraft. *Proc. Institute of Mechanical Engineers, Part G, Journal of Aerospace Engineering*, 213, 131-142. doi: 10.1243/0954410991532909.

Behrouzi, P., & McGuirk, J. J. (2000). Experimental data for CFD validation of the intake ingestion process in STOVL aircraft. *Flow, Turbulence and Combustion*, 64, 233-251. doi: 10.1023/A:1026504202832.

Chuang, S., Chen, M., Lii, S., & Tai, F. (1992). Numerical simulation of twin-jet impingement on a flat plate coupled with cross-flow. *International Journal for Numerical Methods in Fluids*, 14, 459-475. doi: 10.1002/fld.1650140406.

Cox, M., & Abbott, W. A. (1966). Jet recirculation effects in V/STOL aircraft. *Journal of Sound Vibration*, 3, 393-406. doi: 10.1016/0022-460X(66)90105-2.

Daly, B. J., & Harlow, F. H. (1970). Transport equations in turbulence, *Physics of Fluids*, 13, 2634-2649. doi: 10.1063/1.1692845.

Gibson M. M., & Launder B. E. (1978). Ground effects on pressure fluctuations in the atmospheric boundary layer. *Journal of Fluid Mechanics*, 86, 491-511. doi: 10.1017/S0022112078001251.

Knowles, K., & Bray, D. (1991). Recent research into the aerodynamics of ASTOVL aircraft in ground environment. *Proc. Institute of Mechanical Engineers, Part G, Journal of Aerospace Engineering*, 205, 123-131. doi: 10.1243/PIME_PROC_1991_205_250_02

Li, Q., Page, G., & McGuirk, J. J. (2007). Large-eddy simulation of twin impinging jets in a cross-flow. *The Aeronautical Journal*, 111, 195-206. https://dspace.lboro.ac.uk/2134/9499.

McLemore, H., Smith, C., & Hemeter, P. (1970). Generalized HGI Investigation of Large Scale Jet VTOL Type Models. NASA-TN-D-5581.

Ostheimer, D., & Yang, Z. (2012). A CFD study of twin impinging jets in a cross-flow. *The Open Numerical Methods Journal*, 4, 24-34. http://benthamscience.com/open/tonumj/articles/V004/24TONUMJ.pdf.

Worth, N., & Yang, Z. (2006). Simulation of an impinging jet in a crossflow using a Reynolds Stress Transport Model. *International Journal for Numerical Methods in Fluids*, 52, 199-211. doi: 10.1002/fld.1174